Deflection of MeV Electrons by Self-Generated Magnetic Fields in Intense Laser-Solid Interactions

F. Pérez,* A. J. Kemp, L. Divol, C. D. Chen, and P. K. Patel

Lawrence Livermore National Laboratory, Livermore, California 94550, USA

(Received 24 May 2013; revised manuscript received 9 September 2013; published 9 December 2013)

We show that the interaction of relativistic-intensity, picosecond laser pulses with solid targets is affected by the reflected light through the strong currents and 10^4 T magnetic fields it produces. Three-dimensional particle-in-cell simulations, with the axisymmetry broken by a small angle of incidence, show that these magnetic fields deflect the laser-accelerated electrons away from the incident laser axis. This directly impacts the interpretation of electron divergence and directionality in applications such as laser-driven ion acceleration or fast-ignition inertial fusion.

DOI: 10.1103/PhysRevLett.111.245001 PACS numbers: 52.38.−r, 52.65.−y

Laser interaction with solid targets in the relativistic regime (above 10^{18} W/cm^2) creates extreme states of high energy density plasmas, of fundamental interest for warm-dense matter [1–3], plasma astrophysics [4], ion beams [5,6], and fast-ignition inertial confinement fusion [7]. The electron currents driven by the laser exceed megaamperes and create gigagauss magnetic fields in the underdense preplasma preceding solid density [8]. Large-scale magnetic fields may stem from processes such as direct laser acceleration [9], temperature and density gradients, or pressure anisotropy [10,11]. Small-scale magnetic fields are generated by microinstabilities [12,13]. In turn, these fields influence the fast electron energy and angular distributions through small-scale scattering or large-scale deflection [14]. Note that the electron current induces magnetic fields inside the overdense solid plasma through its resistive return current [15,16] but we focus here on the effects in the underdense preplasma.

In this Letter, we use three-dimensional (3D) particle-in-cell (PIC) simulations to study the generation of fast electrons in a realistic oblique-incidence laser-target configuration. We find that the reflected light is intense enough to interact relativistically with the preplasma. It creates currents and magnetic fields that compete with and eventually overcome the effects of the incident laser pulse. The currents accelerated by both incident and reflected lasers interact through the fields they generate. We show that this coupling impacts the angular distribution of laser-accelerated electrons. Even a small incidence angle, often employed in experiments, causes the topology of the fields to change drastically compared to normal incidence, and these fields are powerful enough to deflect MeV electrons away from the laser direction. This effect has not been included in the interpretation of previous experiments.

We detail how the reflected laser light drives a strong electron current that is the dominant source of magnetic fields after a few hundred femtoseconds and leads to a deflection of the forward-going relativistic electrons away from the laser axis. Each stage of the process is compared with analytical estimates. Three-dimensional simulations, carried out using the explicit PIC code PSC [17], featured a $20 \times 30 \times 42$ μm^3 box with 16 cells per micron and 16 particles of each species per cell, and contained an Al plasma slab of maximum density $100 n_c$, where $n_c = \varepsilon_0 m_e (2\pi c)^2/(e\lambda)^2$ is the critical electron density at the laser wavelength $\lambda = 1$ μm. The envelope of the p-polarized laser field was Gaussian with a 3 μm waist, which focuses to $I = 2 \times 10^{19}$ W/cm^2 when in vacuum, with a 16° angle of incidence with respect to the target normal. Its intensity temporal shape was a 0.4 ps full-width-at-half-maximum Gaussian starting at 2% of the maximum intensity, reaching peak power at 600 fs. The density and level of ionization of the preplasma are derived from 2D hydrodynamic simulations relevant to the prepulse energy of the Titan laser system at the Lawrence Livermore National Laboratory. The initial electron density profile is characterized by a double exponential with scale lengths of 1 and 15 μm, the critical density being displaced by 3.5 μm from the target surface. For simplicity, it was chosen transversely uniform, because no noticeable influence of the transverse profile was observed in corresponding 2D simulations. Similarly, collisions were not included after verifying that their role was minimal. Particles are reflected at the laser entrance and absorbed on the other sides. Fields are periodic on the sides and absorbed at the boundary opposite to the laser entrance. To ensure a negligible influence of the boundaries, we ran a series of 2D simulations and verified that changing the box size up to 150×180 μm^2 did not qualitatively modify the results.

These simulations, using slightly oblique incidence relevant to recent experiments on the Titan laser, show that multi-MeV electrons turn away from the laser axis. This deflection is illustrated in Fig. 1 showing electron trajectories turning with respect to the laser direction (macroparticle trajectories were randomly selected among the >5 MeV electrons that reached the solid density region). At early times, electrons accelerated to more than 5 MeV

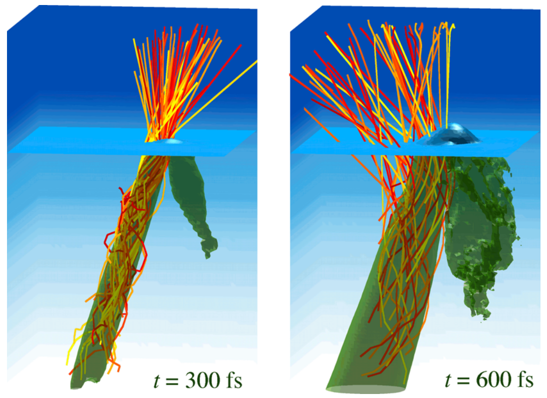

FIG. 1 (color online). Electron deflection in 3D PIC simulation at quarter peak power (left) and at peak power (right). Incident and reflected laser envelopes as green isosurfaces (at intensities 2×10^{18} and 0.4×10^{18} W/cm^2, respectively), fast (>5 MeV) electron trajectories in orange, and target density in blue, with a slice at the critical electron density. The plotted portion is $16 \times 16 \times 30$ μm^3.

are aligned with the laser direction ($\sim 16°$), but they are strongly deflected (up to $-40°$) after 400 fs. The time-integrated angular electron distribution (in both polar and azimuthal angles) is plotted in Fig. 2. Electrons below 5 MeV [see Fig. 2(a)] are distributed evenly around the target normal. The distribution of >5 MeV electrons [see Fig. 2(b)] peaks at $-8°$ and extends to $-40°$. The corresponding divergence half angle is $\sim 15°$ in the incidence plane, and $\sim 6°$ in the transverse direction. Note that this small transverse divergence is related to the laser polarization: we obtained a broader transverse divergence in a simulation with s polarization (the electron deflection effect was still present). In total, 75% of these fast electrons turn further than the target normal, containing 25% of the total electron energy that entered the solid target.

The cause of this deflection is strong magnetostatic fields generated in the underdense preplasma preceding the solid target. The laser stochastically accelerates electrons [18–20] in the region from $0.01n_c$ to $1n_c$ (5 to 30 μm away from the solid target). Electrons directed along the laser axis are continuously accelerated and, thus, form a strong current aligned with the laser, as illustrated in Fig. 3(a). The maximum possible current density along the laser path is $j \sim ecn_e \sim 5 \times 10^{15}$ A/m^2 with a typical electron density $n_e = 0.1n_c$. The displacement current being insignificant on a time scale much larger than the laser period, we can estimate the laser-cycle-averaged magnetic field using Ampère's law $\nabla \times \langle \mathbf{B} \rangle = \mu_0 \langle \mathbf{j} \rangle$. For a laser beam radius of $R = 5$ μm, this creates an azimuthal magnetic field $B = \mu_0 R j/2 \sim 10^4$ T surrounding the beam, clearly visible in Fig. 3(b). It is strong enough to confine multi-MeV electrons inside its path. Example trajectories of such electrons, confined around the laser axis up to the solid target at early times, are plotted in Fig. 1.

At later times, the dominant contribution to the magnetic field is due to the reflected light. The laser reflection is close to specular, the path of the reflected light being symmetrical to the incident one with respect to the target normal. Figure 3(a) shows a stronger current in the path of specularly reflected light, which translates to a stronger magnetic field, as seen in Fig. 3(b). Because the density gradient scale length is sufficiently long (1 to 10 μm) at the interaction region, the reflected light is able to draw a strong current from this dense plasma. Our simulations indicate that 15% of the laser energy is reflected close to the specular direction. Due to scattering and reabsorption, the reflected laser intensity decreases over a few microns, but accelerates "specular" electrons in a large number. These electrons are accelerated to a lower average energy ~ 1 MeV because of the lower light intensity [21], but their velocity remains close to c. Hence, the static magnetic field they induce is stronger than the one due to the incident laser.

This asymmetry between incident and specular paths can be explained by the laser ponderomotive potential evacuating electrons sideways, thus creating a channel, as illustrated in Fig. 4(a). The electron density on the laser path is decreased by a factor 10 at peak power. On the other hand, the intensity of the reflected light is too low to

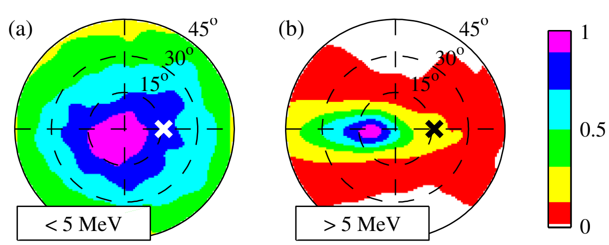

FIG. 2 (color online). Normalized, time-integrated angular distributions of (a) the <5 MeV electrons and (b) the >5 MeV electrons that reach the dense plasma region, in arbitrary units proportional to sr^{-1}. The laser direction is given by crosses and 0° is the target normal.

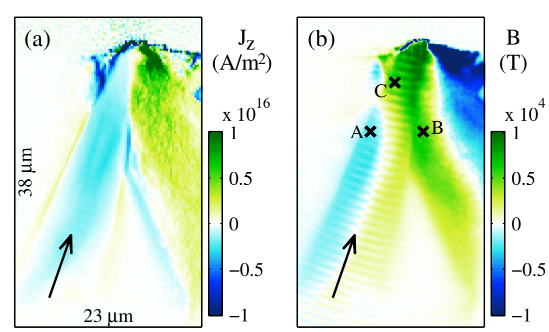

FIG. 3 (color online). 3D PIC simulation results in the incidence plane, at peak power: (a) z component of electron current density and (b) laser-cycle-averaged magnetic field. Arrows indicates the laser direction. The represented box size is given in the figure.

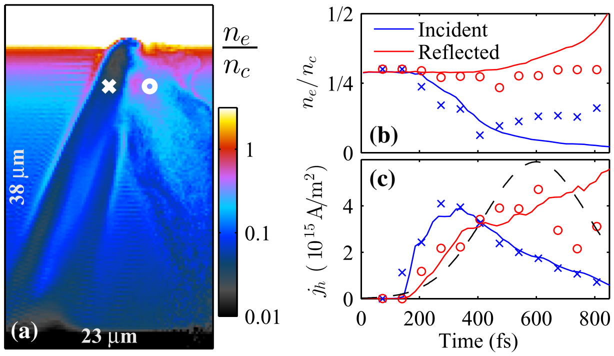

FIG. 4 (color online). Channeling in the 3D PIC simulation at the incidence plane: (a) electron density map at peak power, (b) its time dependence at the points indicated in (a), and (c) the corresponding current. Circles and crosses in (b) and (c) are the models of Eqs. (1) and (2) with $\kappa = 0.16$. Dashed black line: injected maximum laser intensity in arbitrary units.

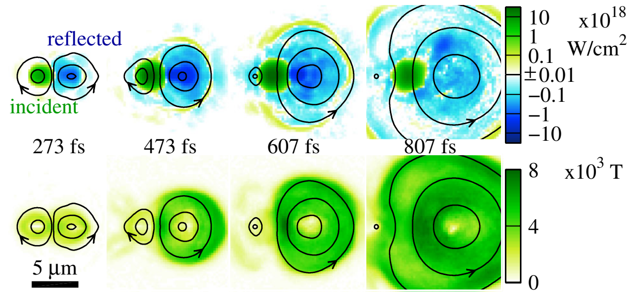

FIG. 5 (color online). Maps from the 3D PIC simulation in a plane parallel to the solid surface (5 μm away). Top row: Poynting flux. Bottom row: magnetic field magnitude. Black lines illustrate a few magnetic field lines.

significantly reduce electron density. This density in the specular path is actually replenished by the plasma pushed away from the laser path. Figure 4(b) shows the time dependence of the electron density n_e inside both the laser path and the specular path (5 μm away from the target surface). We compared this channeling to a known model [22], which, for a Gaussian beam with the intensity envelope $\exp(-r^2/R^2)$, predicts a density variation

$$\frac{\delta n_e}{n_c} = \left(\frac{\lambda}{2\pi R}\right)^2 \frac{a_0^2}{\sqrt{1 + a_0^2}}, \tag{1}$$

where the normalized laser amplitude a_0 is given by $a_0^2 = I\lambda^2 \mu_0 e^2/(2\pi^2 m_e^2 c^3)$. The model is illustrated with markers on Fig. 4(b). Even though Eq. (1) neglects ion motion, which starts to play a role after 500 fs, and the interaction between the incident and specular channels, the good agreement with the simulation results shows that channeling is significant.

Figure 4(c) demonstrates how this change in density affects the currents (solid lines). Before 300 fs, the incident current is 1 to 5 times higher than the specular one. Later, the incident current decreases, matching the density decrease in the channel. On the contrary, no significant channel is formed by the specular light; thus, the specular current does not decrease. As a consequence, the specular current overcomes the incident one after 400 fs.

We have developed a model that reproduces the evolution of these currents due to the variation of the electron density and of the laser intensity. The relativistic electron current density is $j_h \simeq ecn_h$, where n_h is their density. The hot-electron ponderomotive energy from Ref. [21] can be approximated to $T_h \simeq m_e c^2 a_0$ for $a_0 \gg 1$ (note that other studies obtain similar scaling in $\sqrt{I}$; see Refs. [19,23]). Given a laser-to-hot-electron conversion efficiency η, the fast-electron energy flux density $cn_h T_h$ is equal to ηI. Furthermore, assuming that electrons are accelerated independently of each other, the conversion efficiency η is proportional to the background electron density n_e, i.e., $\eta = 2\kappa n_e/n_c$, where we use appropriate normalization and κ as a fitting parameter. Overall, this model leads to a fast-electron current

$$j_h = \kappa ecn_e a_0, \tag{2}$$

and κ is the probability for an electron to be accelerated to a relativistic energy in the path of a laser of amplitude $a_0 = 1$. Figure 4(c) shows that the current (solid lines) is reproduced very satisfyingly by this formula (markers) where intensity and background density vary with time. This confirms that channeling is the key effect responsible for the asymmetry of currents.

Another contribution to the current asymmetry is from the reflected light being spread out at later times. Figure 5 (top row) shows snapshots of the laser Poynting flux in a plane parallel to the target, 5 μm away from the solid surface. The incident laser spot (top, in green) barely changes in size, while the reflected light (top, blue area) evolves from a fairly collimated beam to a wide emission. This widening is likely due to deformation and rippling of the reflecting surface at critical density, also observed in the simulations. The current consequently broadens from a thin beam to a wide cone, which causes the magnetic field from the reflected light to further overcome the incident one, as shown in Fig. 5 (bottom row).

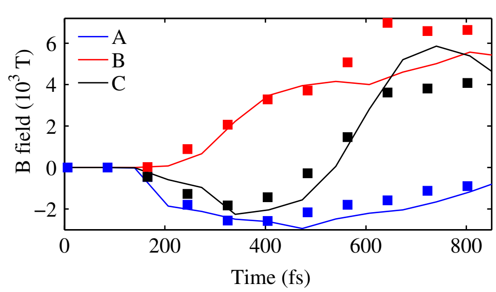

FIG. 6 (color online). 3D PIC simulation magnetic field versus time, at points A, B, and C from Fig. 3(b). Squares illustrate the simple magnetostatics calculation explained in the text.

Figure 6 demonstrates that the magnitude of the magnetic field in the preplasma can be estimated from simple magnetostatics calculations. Modeling the incident and specular currents as two superimposed infinite cylinders of different current densities, we calculated the magnetic fields on points A, B, and C defined on Fig. 3(b) (fields, currents, and cylinder radii were measured versus time in the 3D PIC simulation). Points A and B illustrate the incident and specular contributions, respectively. Point C is representative of the location where fast electrons are deflected, and where magnetic fields are a combination of both incident and specular beams. Figure 6 shows that the magnetostatic model matches well the actual fields. The field at point C matches the contribution from the incident laser (at point A) until 400 fs, and later matches the contribution from the specular light (at point B) because the specular current gradually overcomes the incident one.

As a consequence to this magnetic field evolution, fast electrons traveling within the laser path experience, after peak power, a magnetic field that deflects them away from their initial direction. This explains our observation of an electron beam directed away from the laser axis.

Electrons with smaller energies, between 0.1 and 5 MeV, do not exhibit this turning, and are instead directed in average about the target normal. Their trajectories revealed two kinds of behavior. First, they may originate from the dense region and briefly get to the interaction area where they are accelerated back in the target. Local fields scatter them widely so there is no influence of the laser direction. Second, electrons may gyrate for a while due to the static magnetic fields, eventually reaching the target surface and entering the target with a wide angular distribution. In fact, electrons must have a Larmor radius larger than the lateral extent of the magnetic fields ($\sim 5\ \mu$m) to enter the solid target: this corresponds, in our situation, to an energy >5 MeV.

The electron deflection we describe has not been reported in previous experimental literature even though properties of laser-generated electron beams have been studied in a number of experiments over the last twenty years: their spectrum [24], amount [25], and angular distribution [26] were investigated, as well as how they relate to laser or target parameters [27,28]. A major difficulty is that the signature of these fast electrons can only be found from indirect measurements such as x-ray line emission [29], bremsstrahlung [25], or transition radiation [30]. These indirect data do not completely describe the angular distribution: to infer their average direction and divergence, complex modeling of the measured radiation is required. Consequently, multiple matching situations may be found, which we believe may be the reason for the electron deflection being not inferred before.

As a matter of fact, recent experimental data [31], for which the present study was originally developed, were found consistent with the electron deflection effect. The Titan laser was incident at 16° on a flat 10 μm Al foil backed with a thick Ag slab. Bremsstrahlung emission was collected into detectors at different angles around the target. Comparing with electron transport and bremsstrahlung detection simulations, best agreement was found when the high-energy electron component matched the turning effect described above. When it was set in other directions, such as the target normal or the laser axis, or was even artificially removed, the agreement was not as good.

The mechanism described here requires the specular beam to overlap significantly with the incident one and the reflected light to be intense enough to accelerate strong currents. Indeed, we carried out a series of two-dimensional PIC simulations, which showed that incidence angles larger than 40° and less intense lasers do not show turning electrons. This is consistent with previous experimental results [32–34], which used an incidence angle of 45° and an intensity of $\sim 10^{19}$ W/cm^2. Note that such a large angle of incidence also induces significant refraction: the laser path is bent and may not reach high-enough densities to create strong currents [35].

In conclusion, we explain a new mechanism generating strong magnetic fields in the preplasma and impacting the fast-electron distribution from an intense laser incident on a solid target. 3D PIC simulations show that the reflected laser has a central role: it accelerates moderate-energy electrons ($\sim$MeV) backwards in large number, inducing a $>10^4$ T magnetic field over a large volume. Due to the overlap between incident and reflected light, the forward electrons are strongly deflected by the magnetic field. This is best seen in configurations with nongrazing incidence, significant preplasma, channeling, and reflected light, which are all fairly common characteristics of picosecond-laser interaction experiments. As a consequence, our results may provide new interpretations of such experiments carried out in the past twenty years.

Simulations were carried out on the Livermore Computing Center's Sierra cluster under a LLNL Grand Challenge allocation. This work was performed under the auspices of the U.S. Department of Energy by the Lawrence Livermore National Laboratory under Contract No. DE-AC52-07NA27344.

*perez75@llnl.gov

[1] P. M. Nilson, W. Theobald, J. Myatt, C. Stoeckl, M. Storm, J. Zuegel, R. Betti, D. Meyerhofer, and T. Sangster, Phys. Rev. E79, 016406 (2009).
[2] A. Mančić *et al.*, Phys. Rev. Lett. **104**, 035002 (2010).
[3] Y. Ping *et al.*, High Energy Density Phys. **6**, 246 (2010).
[4] S. J. Moon, S. C. Wilks, R. I. Klein, B. A. Remington, D. D. Ryutov, A. J. Mackinnon, P. K. Patel, and A. Spitkovsky, Astrophys. Space Sci. **298**, 293 (2005).
[5] M. Borghesi, J. Fuchs, S. V. Bulanov, A. J. MacKinnon, P. K. Patel, M. Roth, Fusion Sci. Technol. **49**, 412 (2006).

[6] J. Badziak, Opto-Electron. Rev. **15**, 1 (2007).
[7] M. Tabak, J. Hammer, M. E. Glinsky, W. L. Kruer, S. C. Wilks, J. Woodworth, E. M. Campbell, M. D. Perry, and R. J. Mason, Phys. Plasmas **1**, 1626 (1994).
[8] M. Tatarakis *et al.*, Phys. Plasmas **9**, 2244 (2002).
[9] A. Pukhov and J. Meyer-ter-Vehn, Phys. Rev. Lett. **76**, 3975 (1996).
[10] J. A. Stamper, K. Papadopoulos, R. Sudan, S. Dean, E. McLean, and J. Dawson, Phys. Rev. Lett. **26**, 1012 (1971).
[11] M. G. Haines, Can. J. Phys. **64**, 912 (1986).
[12] A. Bret, L. Gremillet, D. Bénisti, and E. Lefebvre, Phys. Rev. Lett. **100**, 205008 (2008).
[13] A. J. Kemp and L. Divol, Phys. Rev. Lett. **109**, 195005 (2012).
[14] Y. Sentoku, W. Kruer, M. Matsuoka, and A. Pukhov, Fusion Sci. Technol. **49**, 278 (2006).
[15] J. R. Davies, A. R. Bell, M. G. Haines, and S. M. Guérin, Phys. Rev. E **56**, 7193 (1997).
[16] A. R. Bell and R. J. Kingham, Phys. Rev. Lett. **91**, 035003 (2003).
[17] A. J. Kemp, B. I. Cohen, and L. Divol, Phys. Plasmas **17**, 056702 (2010).
[18] J. T. Mendonça and F. Doveil, J. Plasma Phys. **28**, 485 (1982).
[19] A. Pukhov, Z.-M. Sheng, and J. Meyer-ter Vehn, Phys. Plasmas **6**, 2847 (1999).
[20] A. J. Kemp, Y. Sentoku, and M. Tabak, Phys. Rev. E **79**, 066406 (2009).
[21] S. C. Wilks, W. L. Kruer, M. Tabak, and A. B. Langdon, Phys. Rev. Lett. **69**, 1383 (1992).
[22] E. Esarey, P. Sprangle, J. Krall, and A. Ting, IEEE Trans. Plasma Sci. **24**, 252 (1996).
[23] H. Xu, Z.-M. Sheng, J. Zhang, and X.-T. He, Phys. Scr. **77**, 045502 (2008).
[24] H. Sawada, D. P. Higginson, A. Link, T. Ma, S. C. Wilks, H. S. McLean, F. Perez, P. K. Patel, and F. N. Beg, Phys. Plasmas **19**, 103108 (2012).
[25] C. D. Chen *et al.*, Phys. Plasmas **16**, 082705 (2009).
[26] A. Debayle, J. J. Honrubia, E. d'Humières, and V. T. Tikhonchuk, Phys. Rev. E **82**, 036405 (2010).
[27] J. S. Green *et al.*, Phys. Rev. Lett. **100**, 015003 (2008).
[28] S. Chawla *et al.*, Phys. Rev. Lett. **110**, 025001 (2013).
[29] R. B. Stephens *et al.*, Phys. Rev. E **69**, 066414 (2004).
[30] J. J. Santos *et al.*, Phys. Rev. Lett. **89**, 025001 (2002).
[31] C. D. Chen *et al.*, Phys. Plasmas **20**, 052703 (2013).
[32] P. A. Norreys *et al.*, Phys. Plasmas **6**, 2150 (1999).
[33] M. I. K. Santala *et al.*, Phys. Rev. Lett. **84**, 1459 (2000).
[34] B. I. Cho, J. Osterholz, A. Bernstein, G. Dyer, A. Karmakar, A. Pukhov, and T. Ditmire, Phys. Rev. E **80**, 055402 (2009).
[35] R. H. H. Scott *et al.*, Phys. Plasmas **19**, 053104 (2012).